



The brain's hemodynamic response function rapidly changes under acute psychosocial stress in association with genetic and endocrine stress response markers

Immanuel G. Elbau^a, Benedikt Brücklmeier^b, Manfred Uhr^b, Janine Arloth^a, Darina Czamara^a, Victor I. Spoormaker^a, Michael Czisch^b, Klaas Enno Stephan^{c,d,e}, Elisabeth B. Binder^{a,f}, and Philipp G. Sämann^{b,1}

^aDepartment of Translational Research in Psychiatry, Max Planck Institute of Psychiatry, D-80804 Munich, Germany; ^bMax Planck Institute of Psychiatry, D-80804 Munich, Germany; ^cTranslational Neuroimaging Unit, Institute for Biomedical Engineering, University of Zurich and Swiss Federal Institute of Technology Zurich, 8032 Zurich, Switzerland; ^dMax Planck Institute for Metabolism Research, 50931 Cologne, Germany; ^eWellcome Centre for Human Neuroimaging, University College London, London WC1E 6BT, United Kingdom; and ^fDepartment of Psychiatry and Behavioral Sciences, Emory University School of Medicine, Atlanta, GA 30307

Edited by Bruce McEwen, The Rockefeller University, New York, NY, and approved August 14, 2018 (received for review April 6, 2018)

Ample evidence links dysregulation of the stress response to the risk for psychiatric disorders. However, we lack an integrated understanding of mechanisms that are adaptive during the acute stress response but potentially pathogenic when dysregulated. One mechanistic link emerging from rodent studies is the interaction between stress effectors and neurovascular coupling, a process that adjusts cerebral blood flow according to local metabolic demands. Here, using task-related fMRI, we show that acute psychosocial stress rapidly impacts the peak latency of the hemodynamic response function (HRF-PL) in temporal, insular, and prefrontal regions in two independent cohorts of healthy humans. These latency effects occurred in the absence of amplitude effects and were moderated by regulatory genetic variants of *KCNJ2*, a known mediator of the effect of stress on vascular responsivity. Further, hippocampal HRF-PL correlated with both cortisol response and genetic variants that influence the transcriptional response to stress hormones and are associated with risk for major depression. We conclude that acute stress modulates hemodynamic response properties as part of the physiological stress response and suggest that HRF indices could serve as endophenotype of stress-related disorders.

stress | psychosocial stress | functional MRI | hemodynamic response | neurovascular coupling

Stress responses reflect a fundamental process that enables an organism to orchestrate adaptive changes in response to a stressor (1). Central to this process is the hypothalamus–pituitary–adrenal (HPA) axis, a hierarchically organized neuroendocrine system that is activated by actual physical stressors as well as by perceived and anticipated threats, including social evaluation (2). Dysregulation of this process is consistently detected in patients with stress-related disorders such as major depression and post-traumatic stress disorder (3). In addition, both genetic and environmental risk factors for these disorders have been shown to alter the HPA-axis response, suggesting that dysregulation of the stress response may precede and precipitate the development of these disorders (4). Given that interindividual differences in the response to trauma and stress, including psychosocial stress, affect the risk for these disorders (5), there is a continuing need for valid markers of stress vulnerability and resilience at different levels, including the endocrine, molecular, and neural circuit levels.

Combining psychological stress experiments with functional neuroimaging techniques such as fMRI can provide readouts of stress responses at a neural circuit level (6). To date, most studies have described stress-induced neuronal responses in terms of blood oxygen level-dependent (BOLD) amplitudes (7). Overall, these studies, along with comparative functional neuroanatomy (8), suggest that regions regulating the stress response [e.g., hippocampus (HC), anterior cingulate cortex, and ventromedial prefrontal cortex (9)] substantially overlap with regions functionally or structurally altered in major depression (10–16) and even across affective and psychotic disorders (17, 18).

One putative factor that could interlink structural and functional abnormalities in stress-related psychiatric disorders, possibly in both directions, is the control of local brain metabolism through neurovascular coupling (NVC). NVC links neural activity to cerebral blood flow (CBF), thereby dynamically matching metabolic supply to local neural activity. NVC is a fundamental biophysical property of the brain that involves an intricate interplay between neurons, astrocytes, pericytes, and smooth muscle cells (SMC) of their neighboring parenchymal arterioles (for review, see ref. 19). Indeed, recent results from a rodent study have suggested that stress impacts NVC (20). More specifically, subacute behavioral stress impaired vascular responsivity via glucocorticoid receptor (GR)-dependent down-regulation of inwardly rectifying potassium channels (encoded by *KCNJ2*) located on SMCs (20), leading to decreased responsiveness of vascular diameter and thus decreased CBF following neural stimulation. Beyond this relationship between NVC and the HPA axis-controlled endocrine response, there are several points of contact

Significance

Understanding how stress predisposes for psychopathology requires the identification of physiological stress-regulatory mechanisms with pathogenic potential. Here, we applied fMRI to investigate the interaction between acute psychosocial stress and the brain's hemodynamic response function (HRF). The HRF models how local neural activity elicits cerebral blood flow changes, spanning several biophysical processes including neurovascular coupling (NVC). Stress replicably shifted the HRF peak in temporal, insular, and prefrontal brain regions, moderated by functional variants of *KCNJ2*, a protein involved in NVC. Hippocampal HRF markers correlated with the cortisol response and genetic variants that reflect transcriptional responses to glucocorticoids and the risk for depression. We suggest that acute psychosocial stress modulates hemodynamic response properties which could lead to previously undescribed endophenotypes of stress-related disorders.

Author contributions: I.G.E., E.B.B., and P.G.S. designed research; I.G.E., V.I.S., M.C., and P.G.S. performed research; M.U., J.A., D.C., and M.C. contributed new reagents/analytical tools; K.E.S. provided methodological/analytical support; I.G.E., E.B.B., and P.G.S. analyzed data; and I.G.E., K.E.S., E.B.B., and P.G.S. wrote the paper.

The authors declare no conflict of interest.

This article is a PNAS Direct Submission.

Published under the PNAS license.

Data deposition: First-level statistics, commented scripts to generate maps for second-level statistics, individual anatomical parcellations, and cortisol data have been deposited on GitHub (https://github.com/molgen.mpg.de/mpip/Elbau_et_al_PNAS_2018).

See Commentary on page 10827.

¹To whom correspondence should be addressed. Email: saemann@psych.mpg.de.

This article contains supporting information online at www.pnas.org/lookup/suppl/doi:10.1073/pnas.1804340115/-/DCSupplemental.

Published online September 10, 2018.

between NVC and the immediate autonomous nervous system (ANS) response to stress (for a review see ref. 21).

As NVC is critical for the functional and structural integrity of the brain, these findings posit an interaction between stress and NVC as a potential explanation of how prolonged stress could lead to cerebral metabolic changes and structural sequelae and how brain dysfunction and associated psychopathology could be triggered under stressful conditions. There is evidence in mice that pharmacological disruption of NVC leads to cognitive impairment and other neurological dysfunctions (22).

Investigating NVC-related processes in humans directly is currently not possible. However, BOLD fMRI allows one to obtain indices that are sensitive to changes in NVC and other hemodynamic processes. This is not straightforward, as the BOLD response to neuronal activity changes is a complex compound signal, reflecting concurrent contributions from changes in local CBF and volume in different vascular compartments, oxygen utilization, and external physical factors of the MRI system (23–26). One option is to use biophysical models that incorporate physiological parameters, including those that describe NVC processes, from empirical BOLD measurements (25, 27–30). Unfortunately, these models are computationally demanding and presently cannot be used for whole-brain analyses. However, standard mass-univariate whole-brain approaches to human fMRI analysis can be adapted to assess NVC indirectly. Specifically, the canonical hemodynamic response function (HRF), which represents a fixed coupling between neural activity and the subsequent local hemodynamic response in standard convolution models of BOLD data, can be extended by basis functions so that shape deviations from the canonical HRF are flexibly accounted for across voxels (31). In this way, HRF shape descriptors such as HRF peak latency (HRF-PL, “hemodynamic lag”) can be estimated (32). The same model allows the calculation of amplitude responses that are corrected for latency effects (33). While these readouts do not show a unique relation to distinct parameters of biophysically informed NVC models and have limited specificity for disentangling neuronal and vascular contributions to the hemodynamic response (28, 34), this approach can usefully characterize physiological variability of the HRF across subjects and brain regions (35, 36) as well as alterations in etiologically diverse neuropsychiatric conditions such as schizophrenia (37), major depression (38), mild traumatic brain injury (39), and early Alzheimer’s disease (40). Evidence for a genetic component of HRF shape-markers comes from recent twin studies showing a moderate-to-strong heritability of HRF parameters (34).

To our knowledge, no human study has explored the relationship between stress and the brain’s HRF so far. The primary aim of this study was to evaluate whether acute psychosocial stress dynamically modulates HRF shape-markers. To this end, we employed an imaging stress paradigm and tracked HRF-PL as well as latency-corrected HRF amplitudes (33). We then investigated associations between HRF-PL and a common genetic variant regulating *KCNJ2* expression to probe the molecular specificity of these markers with regard to NVC processes as opposed to purely neural processes. Finally, we assessed the relation of stress-related changes in HRF-PL to (i) endocrine stress responses and (ii) genetic variants that alter the molecular response to stress and are associated with risk for major depression (41).

Results

The Psychosocial Stress Paradigm Elicited Effects on Cortisol, Autonomic Nervous System, and Subjective State. To elicit psychosocial stress within the fMRI environment, we utilized a psychosocial stress task (Fig. 1A) that was composed of the same basic elements as the Montreal Imaging Stress Task (42). In principle, it consists of alternating periods of mental arithmetics and rest. During the stress condition, evaluative threat cues (performance assessment, high failure rate, negative verbal feedback) are used to elicit psychosocial stress. In the experimental (EXP) group, to avoid spillover effects and allow tracking of the evolution of stress-related signals, conditions were not

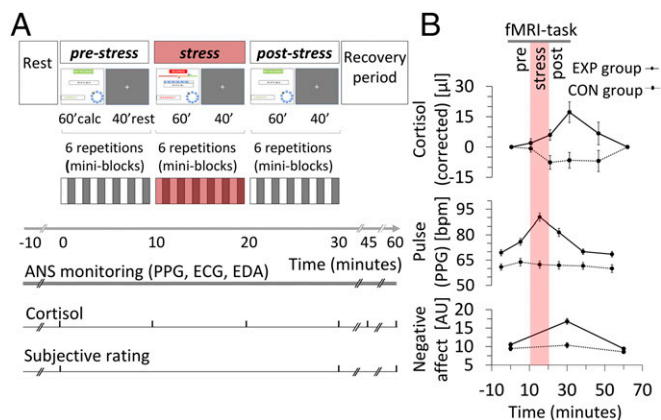


Fig. 1. Overview of experimental design and multilevel stress response. (A) The core fMRI experiment consisted of 10 blocks of mental arithmetics, sectioned into prestress, stress, and poststress periods. Within each period, six blocks of mental arithmetics (~60 s) alternated with rest phases (~40 s). ANS recording was continuous. Blood samples were collected at 0, 10, 20, 30, 45, and 60 min, and subjective ratings were made at times 0, 30, and 60 min. During the recovery period, subjects remained lying on the MRI table but outside the magnet. The stress intervention elicited a marked response at all levels of observation in the EXP group. Panels display estimated marginal means (± 1 SEM) as gained from the repeated-measures ANOVA for both groups. The time window of the stress condition (specific to the EXP group) is indicated by a reddish bar. (B, Top) Note the delayed increase in stress-induced serum cortisol (corrected for circadian drift and baseline offset). (Middle) There is a steep immediate stress-induced increase in pulse rate as derived from pulse plethysmography (PPG). (Bottom) Stress-induced increased negative affect (see Results for statistical details). ECG, electrocardiography; EDA, electrodermal activity.

shuffled, but the stress condition was separated between a prestress and poststress condition. To control for baseline scanner-related stress and time-order effects, a control (CON) group underwent the same procedure but with omission of the evaluative threat cues, resulting in three identical conditions. (For consistency with the temporal sequence in the EXP group, these are also referred to as “prestress,” “stress,” and “poststress” conditions.) To evaluate the effectiveness of the imaging stress test (IST), we tested whether cortisol levels, ANS response (pulse rates calculated from pulse plethysmography), and subjective stress ratings [BSKE (Befindensskalierung nach Kategorien und Eigenschaftsworten) questionnaire] were affected by the stress intervention in the EXP group compared with the CON group (Methods).

Over time, cortisol levels, corrected for circadian drift and baseline offset (SI Appendix, Fig. S1), were higher in the EXP group (group-by-time interaction, $F_{4,54} = 4.405$, $P = 0.004$), as were the circadian-corrected and normalized area under the curve (AUC_{corr}) values [EXP group: mean (SD) 0.074 (0.130); CON group: mean (SD) 0.041 (0.107), Student’s t test, $T = 3.402$, $P = 0.001$, Cohen’s $d = 0.966$] (Fig. 1B, Top).

In both groups, pulse rates showed a battlement pattern throughout the paradigm reflecting ANS modulation during periods of mental effort (SI Appendix, Fig. S2). Both collapsed mental arithmetics and rest values demonstrated a steep pulse rate increase in the EXP group attributable to the stress intervention: group-by-time effect $F_{5,53} = 13.922$, $P = 1.1e-8$ (Fig. 1B, Middle) and $F_{5,53} = 9.180$, $P = 2.4e-6$, respectively; mean difference during stress intervention: Cohen’s $d = 2.182$, $P = 6.1e-10$ and Cohen’s $d = 1.943$, $P = 2e-10$, respectively. Post hoc analyses in the EXP group showed a complete recovery during the postintervention resting period compared with the preintervention resting baseline, starting with the first recovery phase. The recovery of the pulse rate, however, was incomplete between the prestress and poststress condition for both collapsed mental arithmetics and rest values ($P = 3.7e-4$ and $1.4e-5$, respectively).

Mood assessments showed strong group-by-time interactions in the experience of acute stress, arousal, and affect were detected

for the negative affect domain as a whole ($F_{2,56} = 11.518$, $P = 6.4e-5$) (Fig. 1*B*, *Bottom*), carried by the subscales agitation and bad temper ($P = 1.5e-5$ and 0.031 , respectively). Positive affectivity showed changes in the opposite direction ($F_{2,56} = 4.614$, $P = 0.014$), carried by the subscale emotional balance ($P = 0.002$). The subscales anxiety and activity showed no group-by-time changes. Post hoc analyses pointed to reversible changes of all measures that showed a group-by-time effect. In essence, the paradigm elicited a strong endocrine, ANS, and subjective stress response.

Task Main Effects on Latency-Corrected BOLD Amplitudes and Effects of Stress. We then identified brain areas with a sufficient amplitude response to our task effect of interest (mental arithmetics) which is a prerequisite for valid HRF-PL estimations (32). We calculated latency-corrected amplitudes for this filtering step (*Methods*), as amplitudes are underestimated when there is a strong divergence from the canonical HRF-PL of 5 s (33).

During mental arithmetics in the prestress condition, after adequate denoising to control for artifacts due to condition-specific changes in physiological parameters such as heart rate, blood pressure, and respiration (*Methods*), we found expected BOLD activations (in the bilateral intraparietal sulcus, dorsal anterior cingulate cortex, adjacent supplementary motor area, and primary and secondary visual cortex) and deactivations (in the posterior cingulate/precuneus, bilateral parietal cortex, dorsomedial prefrontal cortex, and the HC) matching default mode areas (Fig. 2*A* and *SI Appendix*, Table S1).

The stress intervention enhanced both activations (eight clusters) and deactivations (two clusters) (*SI Appendix*, Fig. S3*A* and Table S2). No significant clusters outside the original (i.e., prestress) regions of deactivation or activation were detected in the stress condition.

Acute Psychosocial Stress Increased HRF-PL in Hippocampal, Insular, and Prefrontal Brain Areas. Our primary interest was to characterize the effect of acute stress on the brain's HRF. As an approximation of this effect, we calculated HRF-PL, an established task-fMRI-based marker (37, 39, 40) that is sensitive to NVC processes linking neural activity to the hemodynamic response (31, 32). While its parallel sensitivity to changes in neuronal responses precludes an interpretation of HRF-PL changes as pure NVC changes (31, 32), this is not a critical limitation for a stress experiment, given that cerebral mediators of fast stress responses such as noradrenaline impact both neuronal and interlinked hemodynamic processes (21,

43). Voxelwise HRF-PL values were calculated from the same model used for the amplitude maps, using estimates for the canonical mental arithmetics regressor and its temporal derivative (*Methods*). This principle was applied to all three conditions, resulting in condition-specific maps of HRF-PL in units of seconds. For the prestress condition, these voxelwise HRF-PL maps revealed a marked regional variability, with group HRF-PL averages between 3.9 s and 6.5 s (Fig. 2*B*), similar in range and distribution to previous reports (37).

We then focused on the main question, i.e., what are the effects of the stress intervention on HRF-PL? A differential, undirected F-test comparing the prestress with the stress condition in the EXP group revealed eight whole-brain-corrected clusters located in the (i) right insula, (ii) left insula and adjacent left inferior ventrolateral cortex, (iii) right inferior ventrolateral cortex, (iv) left insula and superior temporal gyrus, (v) right HC bordering the amygdala and putamen, (vi) left HC, (vii) left supplemental motor area, and (viii) left inferior ventrolateral cortex (Fig. 3 and Table 1). Contrast plots of peak voxel parameter estimates (Fig. 3) allowed further qualitative observations: (i) All changes represented HRF-PL increases; (ii) the stress-induced shifts of HRF-PL showed a marked backswinging in the poststress condition; and (iii) the CON group showed no such changes in HRF-PL between the prestress and stress condition. These clusters that showed that a stress-induced HRF-PL increase did not overlap spatially with the clusters that showed stress-induced BOLD amplitude changes (see combined 3D rendering, *SI Appendix*, Fig. S3*B*). The specificity of the HRF-PL changes regarding the experimental intervention was further demonstrated by statistical comparisons that involved the CON group: (i) Contrast values of all eight EXP group-based clusters showed Bonferroni robust group-by-time effects ($P = 1.1e-05-0.0057$); (ii) within the CON group, no condition-specific effects were found in the respective differential F-contrast (prestress vs. stress); and (iii), more importantly, the direct group comparison in terms of an anatomically unconstrained test for group-by-time interactions (t test, $P_{\text{voxel}} < 0.001$, whole-brain-corrected cluster inference) confirmed an interaction pattern for six of eight clusters. Taking these results together, we found a marked, dynamic, and reversible effect of acute stress on HRF-PL in the HC as well as in insular, lateral temporal, and ventral prefrontal brain regions within a short period of seconds to minutes, spatially dissociated from the BOLD amplitude response to stress. To allow a higher degree of generalizability, all secondary correlations between HRF-PL and independent physiological measures (genetic, ANS, or endocrine information) were performed on regional HRF-PL values derived from individual high-resolution image-based anatomical segmentations (80 parcels) (*Methods*).

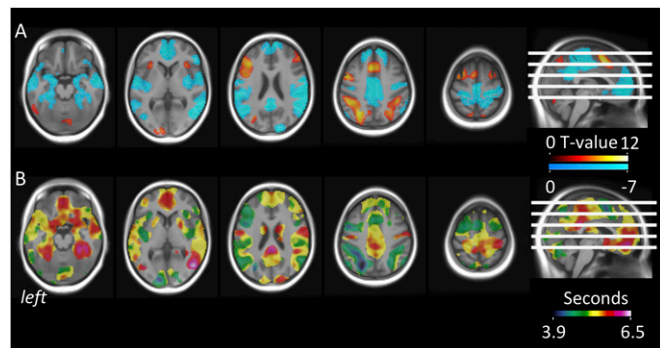


Fig. 2. BOLD amplitude effects and regional variability of HRF-PL during mental arithmetics. (A) Group-level estimates of positive (hot) and negative (cold) BOLD amplitude effects of mental arithmetics in the absence of stress (prestress condition). Amplitude effects are modeled in a first-level GLM including the canonical HRF (β_1) and its temporal derivative (β_2) and are corrected for latency-induced amplitude bias. All reported clusters are significant at $P_{\text{cluster, FWE}} < 0.05$ (collection threshold $P_{\text{voxel}} < 10e-4$). (B) Voxelwise group-level estimates of HRF-PL values in seconds, as computed from sigmoid-transformed β_2/β_1 ratios (*Methods*). The bright transparent overlay marks areas with sufficient overall BOLD response for valid peak latency estimation.

Genetic Variation in *KCNJ2* Expression Correlated with Stress-Related HRF-PL.

Given the inherent ambiguity of HRF-PL with regard to neuronal and vascular processes, we sought to test whether stress-related changes in HRF-PL and stress-related changes in NVC in animals were influenced by similar molecular mechanisms. To this end, we investigated whether HRF-PL values were influenced by *KCNJ2* expression levels. *KCNJ2* has been shown to mediate the effects of stress on NVC in rodents (20). For these analyses, we made use of an expression quantitative trait locus (eQTL) for *KCNJ2*, the SNP rs3848453. This genetic variant explains a substantial proportion of the expression variance in skeletal muscle cells (*SI Appendix*, Fig. S4) that is robust to correction for multiple testing, with additional nominal or trend-significant effects in SMC-rich tissues such as uterus, esophagus, and tibial artery. Correlating the number of C alleles for rs3848453, which is associated with higher *KCNJ2* expression, with all 80 regional HRF-PL values from the prestress and stress conditions led to two main observations. First, the strongest nominal association was detected during the stress condition (right temporopolar cortex, $P = 0.00058$), robust to multiple test correction within the condition ($P_{\text{corr, stress}} = 0.038$) and at trend level across conditions ($P_{\text{corr, both}} = 0.069$). Second, using permutation analysis, we noted a regional expansion of the nominally significant associations for rs3848453 from a

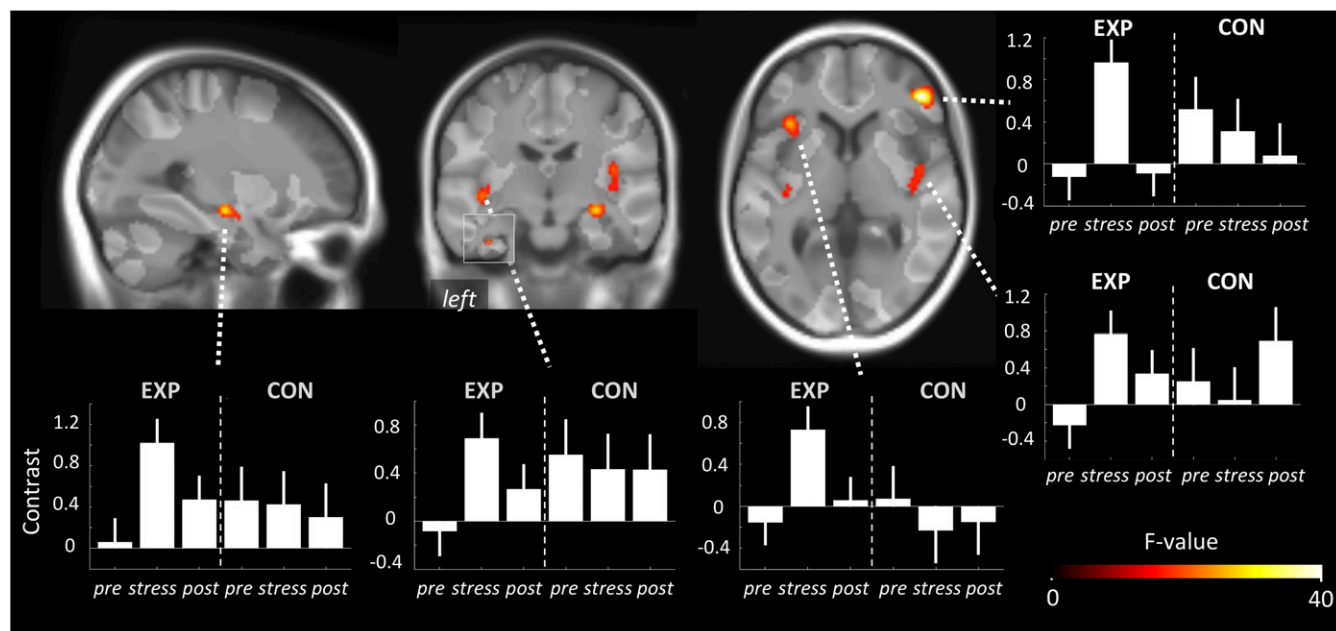


Fig. 3. Effect of stress condition on HRF-PL. Sagittal, coronal, and axial projections on the group template depicting whole-brain significant clusters in which HRF-PL differed in the prestress and stress conditions in the EXP group (undirected F-test; $P_{\text{cluster,FWE}} < 0.05$; collection threshold $P_{\text{voxel}} < 10e-4$). Graph bars represent the mean HRF-PL for peak voxels of these clusters throughout the three conditions for the EXP group and CON group. Note the reversible deflection during stress specifically within the EXP group. Importantly, this analysis was unconstrained by any hypothesis about the HRF-PL of the poststress condition. The bright transparent overlay marks areas with sufficient overall BOLD response for peak latency estimation.

midline-posterior pattern (11 regions) toward a prefrontal-temporal pattern (19 regions in total), with both the number of associated regions in the stress condition and the increase of associated regions exceeding chance probability ($P = 0.008$ and $P = 0.039$, respectively). All 19 regions showed increasing correlation strengths compared with the prestress condition, and 12 were specific to the stress condition, including the right HC, bilateral rostral anterior cingulate cortex, and medial orbitofrontal cortex (Fig. 4A). Given the specific preclinical experimental evidence of a relation between *KCNJ2* expression and NVC changes, these data support the notion that stress-associated

HRF-PL changes may reflect, at least in part, stress-induced changes in NVC.

The HC HRF-PL Response Is Associated with the Endocrine Stress Response. To understand whether these HRF-PL changes were functionally coupled to the endocrine response level, we investigated how stress-induced HRF-PL changes relate to our cortisol marker (cortisol AUC_{corr}). For these secondary analyses, we focused on anatomical regions with a minimum 10% spatial overlap with clusters indicating a significant stress-induced HRF-PL change (Methods, Table 1, and SI Appendix, Fig. S6A).

Table 1. Regional HRF-PL results and correlation of HRF-PL with cortisol response and polygenic differences in the transcriptional response to GR activation (PGS)

Cluster no.*	FreeSurfer location [†]	Mean HRF-PL (SD)		Correlation [‡] of HRF-PL with cortisol AUC_{corr}		Correlation [‡] of HRF-PL with PGS	
		Prestress	Stress	Prestress	Stress Δ	Prestress	Stress Δ
1	R insula	5.171 (0.601)	5.722 (0.392)	n.s.	n.s.	0.432 (0.008)	n.s.
2	R IFG (pars triangularis)	5.055 (0.577)	5.498 (0.557)	n.s.	n.s.	n.s.	n.s.
3	L IFG (pars triangularis)	5.129 (0.620)	5.390 (0.730)	n.s.	n.s.	n.s.	n.s.
	L insula	5.017 (0.576)	5.544 (0.491)	n.s.	0.375 (0.019)	0.394 (0.018)	−0.351 (0.036)
4	L insula	5.017 (0.576)	5.544 (0.491)	n.s.	0.375 (0.019)	0.394 (0.018)	−0.351 (0.036)
	L STG	5.349 (0.551)	5.630 (0.454)	−0.349 (0.029)	n.s.	0.402 (0.015)	n.s.
5	R amygdala	5.439 (0.739)	5.922 (0.616)	n.s.	n.s.	n.s.	n.s.
	R hippocampus	5.470 (0.738)	5.707 (0.493)	−0.493 (0.001) [§]	0.458 (0.003) [§]	0.538 (7e-4) [§]	−0.373 (0.025)
	R putamen	5.604 (0.800)	5.970 (0.634)	−0.353 (0.027)	0.323 (0.045)	0.457 (0.005)	n.s.
6	L hippocampus	5.404 (0.605)	5.774 (0.510)	−0.287 (0.080)	n.s.	0.306 (0.070)	n.s.
7	L SFG	5.060 (0.418)	5.418 (0.226)	n.s.	n.s.	n.s.	n.s.
8	L IFG (pars opercularis)	5.830 (0.716)	5.271 (0.627)	n.s.	n.s.	n.s.	n.s.

IFG, inferior frontal gyrus; ITG, inferior temporal gyrus; L, left hemispheric location; n.s., not significant; R, right hemispheric location; SFG, superior frontal gyrus; STG, superior temporal gyrus; Stress Δ , stress – prestress.

*Cluster number according to SPM results as tabulated in SI Appendix, Table S1.

[†]Corresponding cortical regions according to FreeSurfer parcellation. Note the double appearance of left insula that overlaps with clusters no. 3 and no. 4.

[‡]Pearson r (P values).

[§]Robust to Bonferroni correction for 11 regions.

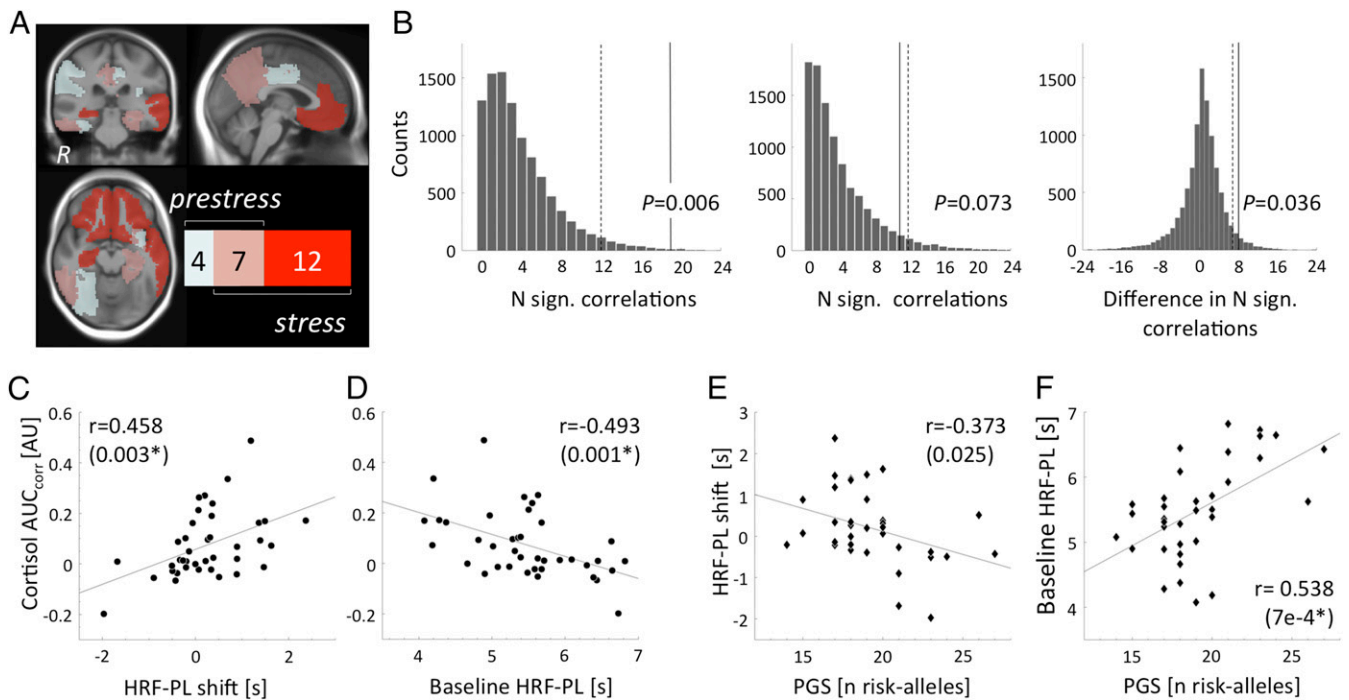


Fig. 4. Functional characterization of HRF-PL effects using *KCNJ2* eQTL, polygenic differences in the transcriptional response to GR activation (PGS; see color scale), and cortisol. (A) The regional expansion of *KCNJ2*-eQTL (rs3848453) (*SI Appendix, Fig. S4*) vs. HRF-PL association in the EXP group under stress from a midline posterior pattern (11 regions) toward an insular–prefrontal–temporal pattern (19 regions), 12 of which were stress-specific, including the right HC, bilateral rostral anterior cingulate cortex, and medial orbitofrontal cortex. Regional tests were performed using HRF-PL values of individual cortical and subcortical FreeSurfer-based segmentations. For graphical depiction, Montreal Neurological Institute (MNI)-space versions of all regions were combined and overlaid on the study-specific T1 whole-brain average. (B) Distributions of permutation-based *P* values to compare the number of nominally significant (N. sign.) associations for prestress and stress conditions and the difference between conditions. Dashed lines represent chance level of 0.05. (C and D) The right HC HRF-PL shift during stress (stress – prestress) (C) and prestress levels of HRF-PL (D) were significantly correlated with the cortisol response. Note that the y axis is the same in C and D. (E and F) The inverse correlation pattern was observed for HRF-PL shift (E) and prestress HRF-PL (F) with the PGS. In C and E, the HRF-PL shift distribution [range, -1.97 to 2.37 s; mean (SD): 0.24 (0.86) s] was calculated from the entire HC, including its mid- and posterior stress-nonresponsive parts (Fig. 3). Cortisol and PGS values were also correlated with the HRF-PL shift averaged from the SPM result cluster in the anterior HC ($r = -0.416$, $P = 0.008$ and $r = -0.510$, $P = 0.001$, respectively). The asterisk indicates robustness toward Bonferroni correction for all 11 anatomical regions ($P < 0.05/11 \sim 0.00455$).

Investigating these resulting 11 stress-responsive anatomical regions revealed a significant correlation for the HRF-PL change in the right HC under stress ($r = 0.458$, $P = 0.003$) (Fig. 4C) and an inverse pattern for the prestress values, again with the strongest effect for the right HC ($r = -0.493$, $P = 0.001$) (Fig. 4D). Both correlations were robust under Bonferroni correction for all tested regions and remained similar when the corrected peak cortisol value was used instead of the AUC_{corr} . A closer look at the correlation between the right HC HRF-PL shift and cortisol (Fig. 4C) revealed that although there is a significant stress-induced increase in HRF-PL in the voxelwise analysis on the group level (Fig. 3), a proportion of subjects that start with high prestress HRF-PL values showed stress-induced HRF-PL decreases. The pattern as a whole can best be described as the tailoring of HRF-PL toward an individual, stress-specific level with adaptations from both directions carrying the correlation with the endocrine response. Correlations with adrenocorticotropic hormone (ACTH) were in the same direction but did not survive after correction for multiple tests. The same analyses conducted with latency-corrected BOLD amplitude values revealed no significant correlation. Additionally, correlations with latency-corrected BOLD amplitudes were significantly weaker than with HRF-PL (Hotelling's test, $P = 7e-4$). Taken together, a strong relationship between HRF-PL dynamics under stress specifically in the right HC and stress-induced cortisol secretion was detected that was absent for BOLD amplitude markers.

The Duration and Magnitude of the HC HRF-PL Response over the Experiment Predicted the Endocrine Response. To better understand the dynamics of HRF-PL evolution and backswing during

and after stress, we applied a temporally finer-grained model that allowed tracking HRF-PL values over 18 blocks, each corresponding to 60 s of mental arithmetics. Fig. 5A depicts the development of right HC HRF-PL values gained from this model that revealed a prompt and steep increase of HRF-PL by about 0.6 s. This increase occurred within the first block (60 s) of the stress condition and gradually returned to baseline during the poststress period.

To characterize the temporal order of HRF-PL changes in cortisol and ACTH secretion, we explored which time window (starting with block no. 4 through block no. 18, with all possible combinations of contiguous blocks) provided the best prediction of cortisol and ACTH AUC_{corr} response. The average of the first three blocks of the control condition were defined as baseline. For cortisol AUC_{corr} , the correlation was highest for the HRF-PL response stacked between blocks no. 7 and no. 16 (i.e., starting with the stress condition and reaching into two-thirds of the poststress condition) (Fig. 5C). For ACTH, the highest correlation was found for an earlier window between blocks no. 6 and no. 11 (i.e., starting with the last block of the prestress condition and including almost the entire stress condition) (Fig. 5B). Together, these results illustrate that both the duration and magnitude of the HC HRF-PL response were associated with the endocrine response. Given the similarity between HRF-PL in the fine-grained model and pulse rate changes (*SI Appendix, Fig. S2*) at the group level, we performed additional analyses to confirm that stress-related HRF-PL effects were not secondary to parallel vascular effects of the sympathoadrenergic activation (*SI Appendix, Fig. S5*).

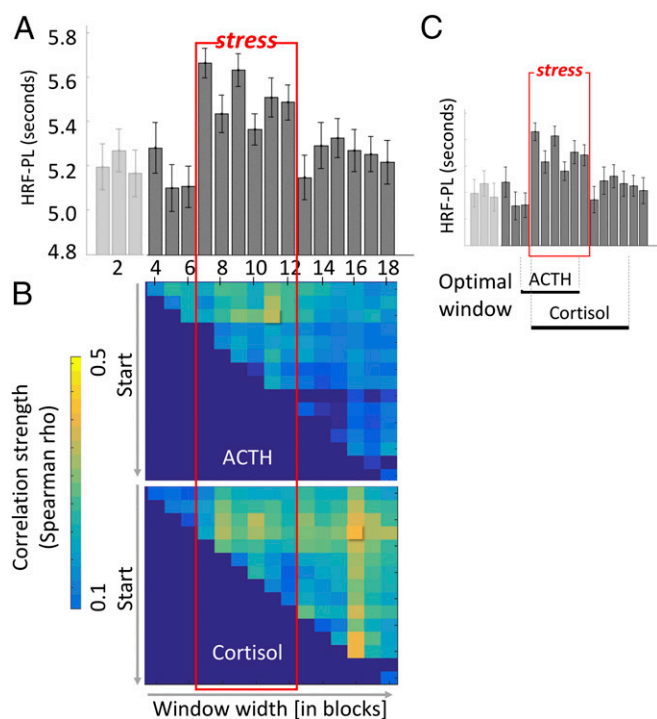


Fig. 5. Trajectory of right HC HRF-PL and dynamic prediction of endocrine response. HRF-PL values were estimated from a GLM with 18 separately modeled blocks (prestress blocks 1–6, stress blocks 7–12, poststress blocks 13–18), and mean values were extracted from individual atlas parcels of the right HC. (A) In the EXP group, a sharp increase with the onset of the stress condition (red box) and a gradual decline during the poststress condition are seen. No such pattern is detectable within the CON group. (B) Exploration of the time span (varying starting block and time window width) with maximal prediction of the stress-induced cortisol (Upper) and ACTH (Lower) response. (C) Black horizontal bars below the graph mark the maximal prediction of cortisol for time window blocks nos. 7–16, reaching into the poststress condition, and of ACTH for time window blocks nos. 6–11.

HC Baseline HRF-PL and Stress-Related Shift Were Predicted by the Polygenic Score of the Molecular Stress Response. To extend these results from acute stress regulation to a trait marker of molecular stress responsiveness, we tested whether polygenic differences in the transcriptional response to GR activation (polygenic score, PGS) that have previously been associated with risk for major depression and differences in amygdala activation (41) also impacted HRF-PL changes with stress. For this, we first assessed how the PGS related to the endocrine and pulse rate response to the stressor, finding a negative association of the PGS with the cortisol response ($r = -0.363$, $P = 0.030$) and no association between the PGS and pulse rate values for the prestress and stress condition and prestress/stress differences.

Correlational analysis for the 11 anatomical regions with significant stress-related HRF-PL increases revealed associations between PGS values and HRF-PL for both stress-induced HRF-PL change ($r = -0.373$, $P = 0.025$) (Fig. 4C and Table 1) and the baseline HRF-PL of the right HC ($r = 0.538$, $P = 7.1e-04$) (Fig. 4D and Table 1), the latter correlation being robust to Bonferroni correction ($P_{\text{corr}} = 0.0078$). As in the cortisol analyses, there was no significant correlation between the PGS and latency-corrected BOLD amplitudes, and correlations of the PGS with HRF-PL and latency-corrected BOLD amplitudes were significantly different (Hotelling's test, $P = 0.008$). Taken together, these findings suggest that prestress HRF-PL of the right HC is influenced by genetic differences predicting GR-induced gene transcription that are also associated with risk for stress-related brain disorders.

Integrating GR Regulatory Genes, Stress-Induced HC HRF-PL Changes, and Endocrine Response. An inverse correlation between genomic determinants of transcriptional GR sensitivity and the cortisol response to a stressor is plausible, as individuals with higher molecular sensitivity to GR will require less cortisol release for comparable genomic effects. Given the continuous feedback mechanisms of the stress-hormone system, such interindividual variation in transcriptional effects of GR activation may have long-term consequences on brain functions that adjust the set point of the HPA-axis response. The HC plays a central role in HPA-axis regulation (8), and correlations between human HC markers and cortisol levels are well established (6, 44, 45). Our results suggest that genetic differences in GR sensitivity could influence stress-induced hemodynamic response properties of the hippocampus to adjust its control of cortisol response to the individual susceptibility. Fig. 6 outlines an observation-based framework that integrates genetically determined GR sensitivity, HC HRF-PL baseline and shift, and cortisol release. In a mediation analysis, we tested the degree to which HC HRF-PL estimates accounted for the influence of PGS on cortisol release, finding a significant indirect contribution of prestress right HC HRF-PL as a mediator [permutation analysis ($n = 10,000$): indirect effect: -0.010 , 95% CI (-0.027 ; -0.001), $P < 0.001$; effect size v : 0.050 , 95% CI (0.006 ; 0.189)]. A similar effect was detected for the stress-induced HC HRF-PL change [-0.006 95% CI (-0.016 ; -0.001), $P < 0.05$; effect size v : 0.020 95% CI (0.001 ; 0.088)]. Both effects are likely specific to the HC, given that HRF-PL vs. cortisol release and PGS correlations were selective for this region after strict correction for multiple testing.

Effects of Stress on HRF-PL Were Replicated in an Independent Sample.

To assess the robustness of regional HRF-PL changes during stress, we investigated an independent sample of 39 healthy subjects using a practically identical multimodal stress paradigm and identical data-processing steps (Methods). First, we compared the similarity of the neuroanatomical pattern of stress-induced HRF-PL shifts between the original and the replication sample at both the voxel and the segmentation-based regional level. Fig. 7A shows whole-brain significant clusters with a stress-induced HRF-PL change in the replication sample, exhibiting a similar effect focus in bilateral insular and superior temporal cortices (SI Appendix, Table S4). With regard to the effect directions, all detected clusters reflected an HRF-PL increase under stress and regressed in the poststress condition, as in the original sample and as exemplified in Fig. 7A. The regional stress-induced HRF-PL values indicated an average general right-shift under stress (SI Appendix, Fig. S84); more specifically, there was a linear correlation of the spatial distribution of these shifts in both samples ($r = 0.585$, $P = 1.9e-08$) (Fig. 7B). Most regions containing significant clusters in the original voxel-based analysis were located close to the regression line. Beyond this, the regional analysis approach, by its multivoxel aggregation principle, revealed additional temporal and parietal regions with robust HRF-PL increases in both samples. In addition, regional HRF-PL values for the prestress condition were strongly correlated across both samples ($r = 0.734$, $P = 2.0e-14$), demonstrating a general replicability of the spatial prestress HRF-PL pattern (SI Appendix, Fig. S8B).

Discussion

Our results demonstrate that acute psychosocial stress elicits changes in HRF-PL in HC and insular, temporal, and prefrontal cortices. These hemodynamic lag changes were associated with genetic differences in *KCNJ2* expression, a gene encoding a potassium channel that influences NVC under stress. Furthermore, the HRF-PL shift in the HC, a key HPA-axis regulator, predicted subsequent cortisol release, suggesting that rapid stress-related adaptations of hemodynamic response properties in the HC promote its HPA-axis regulatory function. HC HRF-PL values were also associated with a polygenic marker of transcriptional GR sensitivity, additionally indicating that the processes underlying HC HRF-PL changes are under complex

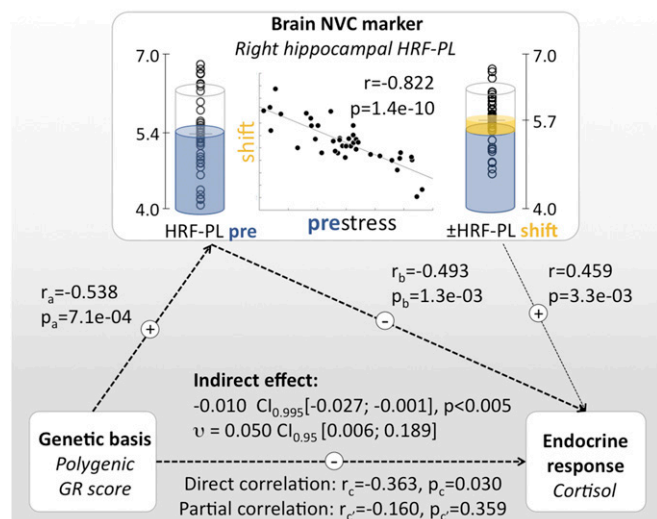


Fig. 6. Integrating polygenic differences in the transcriptional response to GR activation (PGS), HC HRF-PL, and the endocrine response. There are significant correlational links between the PGS, stress-induced cortisol release, and HC HRF-PL values. Note the close inverse relationship between HC prestress HRF-PL and stress-induced HRF-PL shift [central scatter plot and prestress/stress condition-specific data points; see also *SI Appendix, Fig. S7*]. (Left) PGS as static genetic influence. (Center) Baseline HC HRF-PL and stress-induced HRF-PL redistribution. (Right) Endocrine response. Based on the temporal order of observations and known HC functions regarding HPA axis regulation, the degree of a putative mediating role of HRF-PL was probed, revealing a significant indirect effect of HC prestress HRF-PL values. A weaker indirect effect was detected for the HC HRF-PL shift as a mediating variable [−0.006, 95% CI (−0.016; −0.001), $P < 0.05$; effect size ν : 0.020, 95% CI (0.001; 0.088)].

genetic control. Taking these findings together, we posit that hemodynamic lag changes reflect a process that is involved in the individual response to acute stress and might be valuable for assessing how stress sensitivity contributes to the risk for stress-related illnesses.

Spatial Distribution of HRF-PL Changes and Dissociation from Amplitude Effects. The majority of regions that showed stress-induced HRF-PL changes previously have been shown to be involved in regulating the stress response. Of these, the HC and the amygdala are most strongly implicated in regulating HPA-axis responses, primarily by interrupting inhibitory input to the hypothalamic paraventricular nucleus (8). The amygdala, important for salience monitoring and fear processing (46), conveys fast input to hypothalamic nuclei that control the sympathetic nervous system and to neuromodulatory nuclei regulating the cholinergic (nucleus basalis of Meynert), noradrenergic (locus coeruleus), and dopaminergic (ventral tegmental area) tone (47). Regions showing stress-induced HRF-PL shifts also included the bilateral insula, a primarily viscerosensitive region with important functions for interoception (48), modulation of cardiac functions (49), and integrating homeostatic incongruence with the generation of emotional states (50). Finally, the ventrolateral prefrontal cortex has been proposed to serve as a modulator of stress perception and stress response through executive functions (9), enabling down-regulation of the cortisol response (51). Given the close relation of psychosocial stress with the cognitive task in the IST, it is of note that a HC–insula–prefrontal pattern was found only for HRF-PL but not for BOLD amplitude effects (*SI Appendix, Fig. S3B*).

Specificity of the HRF-PL Changes and Synopsis with *KCNJ2* eQTL Analysis. While the sensitivity of our fMRI analyses to condition effects was optimized by a repeated-measures study design

that reduces subject- and region-specific variation of HRF (36, 52), the specificity of the observed HRF-PL/amplitude pattern is limited. On the one hand, simulations based on a biophysically interpretable hemodynamic model illustrated that HRF-PL is most sensitive to parameters of NVC delay and, to a lower degree, transit time (time to transverse the venous compartment) (34), whereas manipulation of other parameters had less influence on HRF-PL and were paralleled by amplitude changes. On the other hand, the interpretation of HRF-PL changes is ambiguous, as emphasized in the original conceptualization of this marker (31, 32). In particular, HRF-PL cannot, on its own, disentangle changes in the timing of neuronal activity from changes in NVC. Thus, scenarios remain in which a neuronal contribution to the HRF-PL effect is well conceivable, e.g., a mismatch between the modeled stimulus timing and the actual neuronal response or an altered stimulation pattern under stress with subsequent interferences between consecutive BOLD responses (see *SI Appendix* for additional details and discussion).

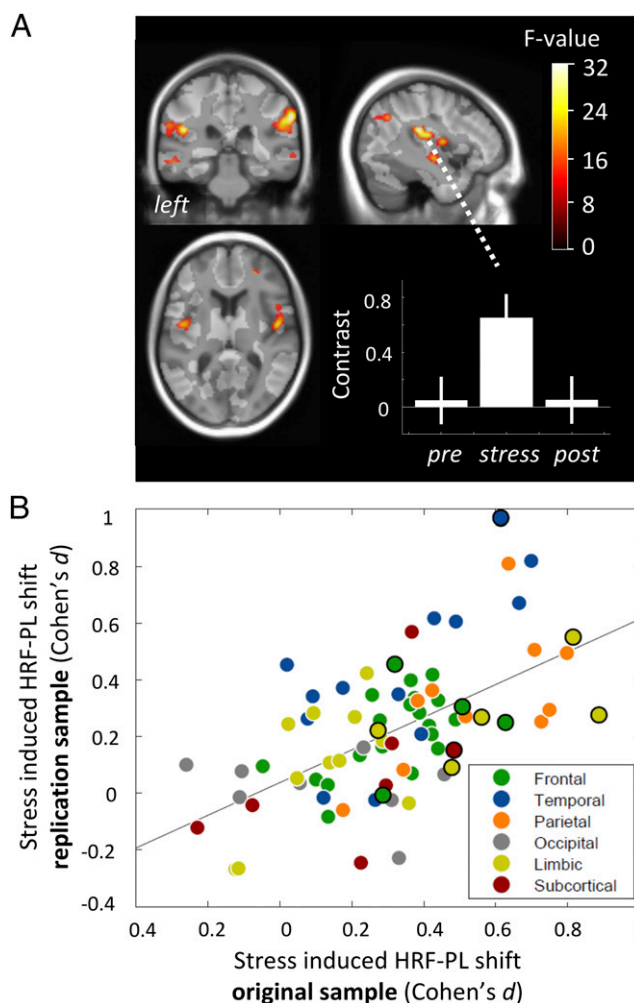


Fig. 7. Overview on replication results. (A) Voxel-based analysis with statistical map of F-value contrast comparing prestress and stress conditions in the replication sample, showing equally directed and reversible HRF-PL increases in bilateral insular, superior temporal, parietolateral, and right orbitofrontal cortices (collection threshold $P < 0.001$, six significant whole-brain corrected clusters, $P_{\text{cluster, FWE}} < 0.05$; for details see *SI Appendix, Table S4*). (B) Correlation of regional HRF-PL shift effects between samples, calculated from voxels with sufficient latency-corrected BOLD amplitude responses in individual anatomical parcellations ($r = 0.585$, $P = 1.9e-08$). Black circles denote atlas regions that showed an HRF-PL shift in the SPM analysis in the original sample (Table 1).

To further address this interpretational ambiguity, we extended our analyses to a genetic marker with molecular specificity to NVC processes in a stress context. One central element of NVC, the dilatation of arterioles, is moderated by inwardly rectifying potassium channels located in vascular SMCs (53). Of relevance to our approach, among the vascular potassium channels involved in astrocyte/SMC signaling, a rodent model of subacute stress has specifically implicated Kir2.1 (orthologous gene *KCNJ2* in humans) as a stress- and GR-dependent NVC regulator (20). In this model, stress caused a glucocorticoid-mediated decrease in functional potassium channels in myocytes, rendering arterioles less responsive to potassium released from astrocytic endfeet and ultimately impairing the hemodynamic response. Using imaging genetics, we showed that genetically determined differences in *KCNJ2* expression were associated with HRF-PL specifically during the stress condition. These findings support an interpretation that our findings on stress-related HRF-PL changes reflect, at least in part, NVC-related processes. However, we acknowledge that the fMRI data do not allow definite conclusions in this regard. Additional studies including neurophysiological measurements are needed to disentangle the neuronal and vascular sources of HRF shape changes in more detail.

Connecting the HC HRF-PL Response with the Endocrine Response. Our observation that HC HRF-PL shift was associated with cortisol secretion (Fig. 4) suggests that one function of the changes in hemodynamic lag under stress might be to promote the adjustment of the HPA axis. We observed a fast onset (~60 s) of HC HRF-PL shifts that, at least in the first 10–15 min, are unlikely to depend on changes in circulating cortisol levels. A sliding-window technique was then employed (Fig. 5) to identify time windows of HRF-PL changes most correlated with the endocrine response. These located to the early stress phase for ACTH and to the entire stress intervention phase, even extending into the poststress phase, for cortisol. As correlations with cortisol would be expected in earlier time windows if the HC HRF-PL were influenced mainly by prestress cortisol, we propose that fast, stress-triggered changes in hemodynamic response properties accompany and potentially promote the HPA axis-regulatory functions of HC neurons. In contrast to HRF-PL, cortisol release was not predicted by stress-induced latency-corrected BOLD amplitude changes in the HC ($P > 0.05$), which at first seems in contrast to findings of Pruessner et al. (6) who reported that stress-induced HC BOLD amplitude decreases correlated with cortisol release. However, when we considered strictly canonical (and not latency-corrected) BOLD amplitudes, we indeed identified weak correlations between HC BOLD amplitudes and cortisol release ($r = 0.396$, $P = 0.013$). This illustrates that in tasks with HRF-PL changes, canonical BOLD amplitude measures may encompass HRF shift effects, thus requiring models that correct for latency differences.

Integrating Genetic Influences on GR Sensitivity, HC HRF-PL, and the Cortisol Response. HRF-PL values in the right HC were also related to genetic traits that moderate GR-dependent transcriptional changes. To demonstrate this, we used a PGS computed from SNPs that both moderate the transcriptional response of GR-target genes and are associated with major depression in a representative genome-wide association study meta-analysis (41). The respective target transcripts are expressed in the brain and include genes related to proteasome degradation and ubiquitination, histone function, and immune response. The PGS was weighted by the extent to which the alleles moderate the transcriptional response following GR activation. Higher scores denote a higher number of alleles associated with larger GR-induced change, i.e., these individuals would require less cortisol for the same downstream effect of GR. In accordance with this assumption, we found that a higher PGS was associated with lower cortisol release during the IST. This difference in cellular GR sensitivity may also be related to the association of

the PGS with HC prestress HRF-PL, especially since the HC is strongly involved in GR-mediated negative HPA-axis feedback (54). Given the continuous feedback mechanisms of the stress hormone system, differential transcriptional effects of GR activation may have long-term consequences on brain function and adjust the set point of the HPA-axis response. Genetically defined GR sensitivity could thus fine-tune HC hemodynamic response properties, indirectly incorporating the optimal magnitude of cortisol as the feedback signal. In line with this, we observed that stress-induced right HC HRF-PL shifts were dependent on prestress HRF-PL ($r = -0.88$, $P = 1.4 \times 10^{-10}$) (see *SI Appendix*, Fig. S7 for details). Eventually, we found that a small but significant part of the PGS-cortisol variance was explained by HC HRF-PL (Fig. 6), supporting the idea that stress-induced changes in hemodynamic response could be one process that interlinks genetically determined GR sensitivity with the neuroendocrine response.

Rapid Temporal Dynamics of HRF-PL Response: Potential Sources. The rapid dynamics of HRF-PL shifts in response to stress (Fig. 5) raise the question which stress-related regulatory mechanisms could underlie such a temporal pattern. The fast onset of the HRF-PL shift (within seconds) would be compatible with fast neuromodulatory influences on NVC (21) by noradrenergic signals originating from the locus coeruleus (55) as well as cholinergic projections from the basal forebrain (56). Specifically, the locus coeruleus–noradrenaline (LC–NA) network with its widespread, unmyelinated, densely branched neurons can enhance the coupling of blood distribution to local oxygen demands (55), likely by combining global vasoconstriction with local vasodilatory processes (55). Cells associated with the vasculature—i.e., pericytes (57) and astrocytes (58)—are involved in this process, in addition to the effects of norepinephrine on penetrating arterioles through the paravascular space (59). Importantly, the effects of NA on NVC are inseparably entangled with its modulation of neuronal networks (21), and one way in which neuronally triggered NA affects the vasculature relies on SMC inward-rectifier potassium channels (53). In essence, the LC–NA system represents a strong candidate system for explaining stress-associated hemodynamic lag effects, mainly due to its fast action on several NVC components. The LC–NA system previously has been highlighted as putative central counterpart of the peripheral sympathetic nervous system (55), which in our data is reflected in the concordance of pulse rate and HRF-PL trajectories through the experiment (*SI Appendix*, Fig. S2). While this ties into existing stress models that postulate a close interplay between the sympathetic nervous system and the HPA axis (60), the LC–NA network could play a more prominent role in this interplay. So far, NA effects in the paraventricular nucleus of the hypothalamus that lead to corticotrophin-releasing hormone release were believed to originate mostly from medullary catecholaminergic groups rather than from the locus coeruleus (61).

Study Limitations. We observed significantly higher average pulse rates in the EXP group than in the CON group in the prestress condition (*SI Appendix*, Fig. S2), which could indicate different levels of stress anticipation due to imperfect blinding: Subjects in the EXP group were informed during the training phase that an evaluation would occur later, and the experimenter was not blind to group membership, which may have influenced stress anticipation. Despite these factors, however, we observed group-by-time interaction effects on pulse rates, which led us to conclude that the CON group satisfied its purpose in controlling for time effects and unspecific scanning-related stress. A second limitation is the dependency of the HRF-PL estimation methodology used here on experimental conditions (e.g., a cognitive task or sensory stimulation), which precludes investigating HRF features during stimulation-free phases of the paradigm. In fact, the difficulty in replicating the HC HRF-PL shift at the voxel level may have originated from unstable or insufficient deactivation of the HC in the stress condition (*SI Appendix*, Fig. S9). This dependency on

sufficient (de-)activation during a paradigm is currently an inherent limitation in analyzing NVC-related markers by task fMRI. Finally, regardless of the computational approach, HRF shape-markers or the respective parameters estimated from biophysically motivated models of the hemodynamic response (25, 28, 62) face challenges in disambiguating neuronal and vascular responses. This limitation could be overcome by parallel recording of neuronal activity by electrophysiological methods.

Biomarker Perspective. While hemodynamic response abnormalities have been reported in different neuropsychiatric populations (37–40, 63), our study links such processes to acute stress. Different interindividual capabilities in adapting to hemodynamic response properties could contribute to the diversity of subjects' abilities to cope with stress. Beyond this, repeated, chronic, or extreme stressors could lead to lasting changes and maladaptation of the stress response itself or to secondary structural brain changes. Hemodynamic response-related factors could explain the overlap between structural brain changes in stress-related disorders (14, 15, 17), regions undergoing hemodynamic response adaptations under acute stress, and regions coordinating the acute stress response (64). Vascular abnormalities could influence the stress response and thereby link neurovascular risk to the risk of psychiatric disease (65). Hemodynamic response indices could serve as biomarkers of stress-related disorders and, given the heritability of HRF-related markers (34), lead to stress endophenotypes to uncover novel genetic risk variants for stress-related psychiatric disorders.

Methods

Study Sample, Design, and Experiment. The core experiment was performed on 59 healthy subjects who underwent a psychosocial stress experiment, the IST, during fMRI paralleled by endocrine and ANS monitoring. After a thorough check of eligibility and before closer assessment by medical study personal, all subjects were told the outline of procedures, and all participants gave informed written consent to the study protocol that had been approved by the ethics committee of the Ludwig-Maximilians-University, Munich. Subjects were partially blinded for the purpose of undergoing a stress experiment but were informed that they would perform mental arithmetics under different conditions and that in one phase their performance would be recorded and watched by experimenters (*SI Appendix, Supplemental Methods I.1*). Details are given in Fig. 1 and *SI Appendix, Supplemental Methods I.2*. Participants were randomly assigned to EXP ($n = 39$) or CON ($n = 20$) groups that differed by the stress intervention. The IST core part spans 30 min and resembles the Montreal Imaging Stress Task (42), similarly built on evaluative threat to induce stress during mental arithmetics (*SI Appendix, Supplemental Methods I.3*). It consists of 18 blocks of pairs of mental arithmetics (60 s) and rest (40 s) with stress induced during blocks 7–12 by graphical evaluative cues, time constraints, and repeated negative verbal feedback. In the CON group, the stress condition is identical to the prestress and poststress conditions.

MRI Acquisition and Preprocessing. Functional whole-brain echo-planar imaging (EPI) data were acquired on a 3-T MR system along with a single high-contrast EPI and anatomical images (*SI Appendix, Supplemental Methods II.1*). The preprocessing scheme is detailed in *SI Appendix, Supplemental Methods II.2*. A focus was put on combining segmentation of the high-contrast single EPI with DARTEL (66) for optimal intersubject coregistration and on using multiple linear regression to remove effects of regressors reflecting motion and physiological noise [CompCor (67)].

Calculation of Voxelwise HRF-PL Values. First-level models were estimated within the general linear model (GLM) framework of the statistical parametric map (SPM) for the separate prestress, stress, and poststress conditions (see *SI Appendix, Supplemental Methods II.3* for details). All event regressors were convolved with the canonical HRF, and their first derivative was added to the model. HRF-PL maps per subject and condition were calculated following the method of Henson et al. (32) that suggests modelling shifted BOLD responses as linear combinations of the canonically convolved stimulus regressor and its first derivative. For this, the ratio of parameter estimates of the canonical mental arithmetics regressor and its derivative was calculated and submitted to a sigmoid transformation. From the same estimates,

latency-corrected amplitudes (A_{corr}) were calculated (33) for comparative analyses and to define sufficiently activated voxels.

Second-Level SPM Analyses. After proof-of-concept interrogation of task effects on A_{corr} and prestress HRF-PL values (Fig. 2 and *SI Appendix, Supplemental Methods II.4*), the key question—the effects of stress on HRF-PL—was approached using a flexible two-factorial model [two-level factor group (EXP, CON); three-level repeated-measures factor time (equivalent to condition in the EXP group)] (*SI Appendix, Supplemental Methods II.5*). An F-test between prestress and stress was performed in the EXP group to detect stress-dependent HRF-PL changes [cluster defining $P_{\text{voxel}} < 0.0001$; familywise error rate (FWE)-corrected $P_{\text{cluster}} < 0.05$]. *SI Appendix, Supplemental Methods II.6* explains additional analyses of the spatial correlation between effects on HRF-PL and A_{corr} . Reporting of SPM results was based on visual validation and the automated anatomical labeling toolbox (68).

Extraction of Regional HRF-PL Values. For a higher degree of generalizability, all secondary analyses of HRF-PL effects were based on regional values of either a set of 11 disjunct regions responsive to stress (for correlations with cortisol and the PGS) or all 80 FreeSurfer regions (for correlations with a *KCNJ2* eQTL). See *SI Appendix, Supplemental Methods II.7* for the required combined fMRI/anatomical preprocessing and *SI Appendix, Supplemental Methods II.8* for details on the extraction of regional HRF-PL values.

fMRI-Independent Measures.

Endocrine response quantification. Laboratory-related details on cortisol/ACTH measurements are given in *SI Appendix, Supplemental Methods III.1*. Measurements were corrected for circadian trends and normalized to individual average levels, resulting in one AUC_{corr} value for cortisol and ACTH (*SI Appendix, Supplemental Methods III.2*).

ANS signal collection and processing. All associated procedures are reported in *SI Appendix, Supplemental Methods IV.1*. Pulse rates were analyzed at the level of conditions and blocks (*SI Appendix, Supplemental Methods IV.2*) and also are provided as point measurements for inclusion into GLMs.

PGS calculation. Genotyping, imputation, and calculation of the PGS are detailed in *SI Appendix, Supplemental Methods V.1*. In essence, the PGS is constructed from SNPs that reflect differences in the transcriptional response to GR activation and that are associated with major depression (41). **Functional SNP selection for *KCNJ2*.** *SI Appendix, Supplemental Methods V.2* details the selection of an eQTL for *KCNJ2* that had high correlations with expression levels in skeletal and smooth muscle.

Secondary Analyses. Secondary analyses were performed to validate and contextualize the effects of stress on HRF-PL. We first investigated associations between HRF-PL, cortisol, and the PGS (*SI Appendix, Supplemental Methods VI.1*). We then tracked the right hippocampal HRF-PL across the experiment to explore the temporal order of the HRF-PL and endocrine response in greater detail (*SI Appendix, Supplemental Methods VI.2*). After finding co-correlations between these measurements, we performed a mediation analysis to investigate if stress-induced HRF-PL changes can in part explain the PGS/cortisol correlation (*SI Appendix, Supplemental Methods VI.3*). Eventually, to probe the hypothesis that *KCNJ2* influences HRF-PL in humans, we tested the correlations of a specific eQTL of *KCNJ2* with HRF-PL in the prestress and stress conditions (*SI Appendix, Supplemental Methods V.3*).

Replication Analysis. In addition to voxelwise analyses, we investigated if a similar pattern of regional HRF-PL effects can be induced by the same stress experiment in an independent sample (*SI Appendix, Supplemental Methods I.4 and V.4*).

Data and Code Availability. First-level statistics, commented scripts to generate maps for second level statistics, individual anatomical parcellations, and cortisol data have been deposited on GitHub (https://github.com/molgen.mpg.de/mpipj/Elbau_et_al_PNAS_2018). Further requests can be directed to P.G.S. (saemann@psych.mpg.de).

ACKNOWLEDGMENTS. We thank all participants for supporting this project; Neuroimaging Core Unit technicians Ines Eidner, Anna Gallner, and René Schranzer for help in acquiring these data; Anne Kühnel for supporting the validation of fMRI preprocessing; Alina Tontsch and the team of the Max Planck Institute of Psychiatry Biobank for sample processing; the organization team of the Biological Classification of Mental Disorders (BeCOME) study for logistical support; Mark Lachowicz for consulting on the mediation analysis; Bertram Müller-Myhsok for consulting on the permutation analysis; and Sara Kiem for discussions of the design of the imaging stress test.

1. McEwen BS (2000) The neurobiology of stress: From serendipity to clinical relevance. *Brain Res* 886:172–189.
2. Dickerson SS, Kemeny ME (2004) Acute stressors and cortisol responses: A theoretical integration and synthesis of laboratory research. *Psychol Bull* 130:355–391.
3. Vreeburg SA, et al. (2009) Major depressive disorder and hypothalamic-pituitary-adrenal axis activity: Results from a large cohort study. *Arch Gen Psychiatry* 66:617–626.
4. Provencal N, Binder EB (2015) The neurobiological effects of stress as contributors to psychiatric disorders: Focus on epigenetics. *Curr Opin Neurobiol* 30:31–37.
5. Klengel T, Binder EB (2015) Epigenetics of stress-related psychiatric disorders and gene × environment interactions. *Neuron* 86:1343–1357.
6. Pruessner JC, et al. (2008) Deactivation of the limbic system during acute psychosocial stress: Evidence from positron emission tomography and functional magnetic resonance imaging studies. *Biol Psychiatry* 63:234–240.
7. Engert V, Buss C, Pruessner JC (2010) Investigating the association between early life parental care and stress responsivity in adulthood. *Dev Neuropsychol* 35:570–581.
8. Ulrich-Lai YM, Herman JP (2009) Neural regulation of endocrine and autonomic stress responses. *Nat Rev Neurosci* 10:397–409.
9. Dedovic K, Duchesne A, Andrews J, Engert V, Pruessner JC (2009) The brain and the stress axis: The neural correlates of cortisol regulation in response to stress. *Neuroimage* 47:864–871.
10. Anand A, et al. (2005) Activity and connectivity of brain mood regulating circuit in depression: A functional magnetic resonance study. *Biol Psychiatry* 57:1079–1088.
11. Etkin A, Wager TD (2007) Functional neuroimaging of anxiety: A meta-analysis of emotional processing in PTSD, social anxiety disorder, and specific phobia. *Am J Psychiatry* 164:1476–1488.
12. Greicius MD, et al. (2007) Resting-state functional connectivity in major depression: Abnormally increased contributions from subgenual cingulate cortex and thalamus. *Biol Psychiatry* 62:429–437.
13. Kim P, et al. (2013) Effects of childhood poverty and chronic stress on emotion regulatory brain function in adulthood. *Proc Natl Acad Sci USA* 110:18442–18447.
14. Schmaal L, et al. (2016) Subcortical brain alterations in major depressive disorder: Findings from the ENIGMA Major Depressive Disorder Working Group. *Mol Psychiatry* 21:806–812.
15. Schmaal L, et al. (2017) Cortical abnormalities in adults and adolescents with major depression based on brain scans from 20 cohorts worldwide in the ENIGMA Major Depressive Disorder Working Group. *Mol Psychiatry* 22:900–909.
16. Liberzon I, Sripada CS (2008) The functional neuroanatomy of PTSD: A critical review. *Prog Brain Res* 167:151–169.
17. Goodkind M, et al. (2015) Identification of a common neurobiological substrate for mental illness. *JAMA Psychiatry* 72:305–315.
18. McTeague LM, et al. (2017) Identification of common neural circuit disruptions in cognitive control across psychiatric disorders. *Am J Psychiatry* 174:676–685.
19. Petzold GC, Murthy VN (2011) Role of astrocytes in neurovascular coupling. *Neuron* 71:782–797.
20. Longden TA, Dabertrand F, Hill-Eubanks DC, Hammack SE, Nelson MT (2014) Stress-induced glucocorticoid signaling remodels neurovascular coupling through impairment of cerebrovascular inwardly rectifying K⁺ channel function. *Proc Natl Acad Sci USA* 111:7462–7467.
21. Lecrux C, Hamel E (2016) Neuronal networks and mediators of cortical neurovascular coupling responses in normal and altered brain states. *Philos Trans R Soc B Biol Sci* 371:20150350.
22. Tarantini S, et al. (2015) Pharmacologically-induced neurovascular uncoupling is associated with cognitive impairment in mice. *J Cereb Blood Flow Metab* 35:1871–1881.
23. Kim SG, Ogawa S (2012) Biophysical and physiological origins of blood oxygenation level-dependent fMRI signals. *J Cereb Blood Flow Metab* 32:1188–1206.
24. Martindale J, et al. (2005) Long duration stimuli and nonlinearities in the neural-hemodynamic coupling. *J Cereb Blood Flow Metab* 25:651–661.
25. Stephan KE, Weiskopf N, Drysdale PM, Robinson PA, Friston KJ (2007) Comparing hemodynamic models with DCM. *Neuroimage* 38:387–401.
26. Hirano Y, Stefanovic B, Silva AC (2011) Spatiotemporal evolution of the functional magnetic resonance imaging response to ultrashort stimuli. *J Neurosci* 31:1440–1447.
27. Uludağ K, et al. (2004) Coupling of cerebral blood flow and oxygen consumption during physiological activation and deactivation measured with fMRI. *Neuroimage* 23:148–155.
28. Friston KJ, Mechelli A, Turner R, Price CJ (2000) Nonlinear responses in fMRI: The balloon model, Volterra kernels, and other hemodynamics. *Neuroimage* 12:466–477.
29. Havlicek M, et al. (2015) Physiologically informed dynamic causal modeling of fMRI data. *Neuroimage* 122:355–372.
30. Drew PJ, Shih AY, Kleinfeld D (2011) Fluctuating and sensory-induced vasodynamics in rodent cortex extend arteriole capacity. *Proc Natl Acad Sci USA* 108:8473–8478.
31. Friston KJ, et al. (1998) Event-related fMRI: Characterizing differential responses. *Neuroimage* 7:30–40.
32. Henson RNA, Price CJ, Rugg MD, Turner R, Friston KJ (2002) Detecting latency differences in event-related BOLD responses: Application to words versus nonwords and initial versus repeated face presentations. *Neuroimage* 15:83–97.
33. Calhoun VD, Stevens MC, Pearlson GD, Kiehl KA (2004) fMRI analysis with the general linear model: Removal of latency-induced amplitude bias by incorporation of hemodynamic derivative terms. *Neuroimage* 22:252–257.
34. Shan ZY, et al. (2016) Genes influence the amplitude and timing of brain hemodynamic responses. *Neuroimage* 124:663–671.
35. Devonshire IM, et al. (2012) Neurovascular coupling is brain region-dependent. *Neuroimage* 59:1997–2006.
36. Aguirre GK, Zarahn E, D'Esposito M (1998) The variability of human, BOLD hemodynamic responses. *Neuroimage* 8:360–369.
37. Ford JM, Johnson MB, Whitfield SL, Faustman WO, Mathalon DH (2005) Delayed hemodynamic responses in schizophrenia. *Neuroimage* 26:922–931.
38. Gao Q, Zou K, He Z, Sun X, Chen H (2016) Causal connectivity alterations of cortical-subcortical circuit anchored on reduced hemodynamic response brain regions in first-episode drug-naïve major depressive disorder. *Sci Rep* 6:21861.
39. Mayer AR, et al. (2014) Investigating the properties of the hemodynamic response function after mild traumatic brain injury. *J Neurotrauma* 31:189–197.
40. Rombouts SARB, Goekoop R, Stam CJ, Barkhof F, Scheltens P (2005) Delayed rather than decreased BOLD response as a marker for early Alzheimer's disease. *Neuroimage* 26:1078–1085.
41. Arloth J, et al.; Major Depressive Disorder Working Group of the Psychiatric Genomics Consortium (PGC); Major Depressive Disorder Working Group of the Psychiatric Genomics Consortium PGC (2015) Genetic differences in the immediate transcriptome response to stress predict risk-related brain function and psychiatric disorders. *Neuron* 86:1189–1202.
42. Dedovic K, et al. (2005) The Montreal Imaging Stress Task: Using functional imaging to investigate the effects of perceiving and processing psychosocial stress in the human brain. *J Psychiatry Neurosci* 30:319–325.
43. Hall BS, Moda RN, Liston C (2015) Glucocorticoid mechanisms of functional connectivity changes in stress-related neuropsychiatric disorders. *Neurobiol Stress* 1:174–183.
44. Buchanan TW, Tranel D, Kirschbaum C (2009) Hippocampal damage abolishes the cortisol response to psychosocial stress in humans. *Horm Behav* 56:44–50.
45. Pruessner M, et al. (2017) Interplay of hippocampal volume and hypothalamus-pituitary-adrenal axis function as markers of stress vulnerability in men at ultra-high risk for psychosis. *Psychol Med* 47:471–483.
46. Fox AS, Oler JA, Tromp PM, Fudge JL, Kalin NH (2015) Extending the amygdala in theories of threat processing. *Trends Neurosci* 38:319–329.
47. Venkatraman A, Edlow BL, Immordino-Yang MH (2017) The brainstem in emotion: A review. *Front Neuroanat* 11:15.
48. Craig AD (2003) Interoception: The sense of the physiological condition of the body. *Curr Opin Neurobiol* 13:500–505.
49. Oppenheimer S, Cechetto D (2016) The insular cortex and the regulation of cardiac function. *Compr Physiol* 6:1081–1133.
50. Strigo IA, Craig AD (1708) (Bud) (2016) Interoception, homeostatic emotions and sympathovagal balance. *Philos Trans R Soc B Biol Sci* 371:20160010.
51. Wang J, et al. (2005) Perfusion functional MRI reveals cerebral blood flow pattern under psychological stress. *Proc Natl Acad Sci USA* 102:17804–17809.
52. Handwerker DA, Ollinger JM, D'Esposito M (2004) Variation of BOLD hemodynamic responses across subjects and brain regions and their effects on statistical analyses. *Neuroimage* 21:1639–1651.
53. Filosa JA, et al. (2006) Local potassium signaling couples neuronal activity to vasodilation in the brain. *Nat Neurosci* 9:1397–1403.
54. Wang Q, et al. (2013) Glucocorticoid receptor protein expression in human hippocampus; stability with age. *Neurobiol Aging* 34:1662–1673.
55. Bekar LK, Wei HS, Nedergaard M (2012) The locus coeruleus-norepinephrine network optimizes coupling of cerebral blood volume with oxygen demand. *J Cereb Blood Flow Metab* 32:2135–2145.
56. Lecrux C, et al. (2017) Impact of altered cholinergic tones on the neurovascular coupling response to whisker stimulation. *J Neurosci* 37:1518–1531.
57. Mulligan SJ, MacVicar BA (2004) Calcium transients in astrocyte endfeet cause cerebrovascular constrictions. *Nature* 431:195–199.
58. Hillman EMCC (2014) Coupling mechanism and significance of the BOLD signal: A status report. *Annu Rev Neurosci* 37:161–181.
59. Dacey RG, Jr, Duling BR (1984) Effect of norepinephrine on penetrating arterioles of rat cerebral cortex. *Am J Physiol* 246:H380–H385.
60. Andrews J, Ali N, Pruessner JC (2013) Reflections on the interaction of psychogenic stress systems in humans: The stress coherence/compensation model. *Psychoneuroendocrinology* 38:947–961.
61. Pacak K, Palkovits M, Kopin IJ, Goldstein DS (1995) Stress-induced norepinephrine release in the hypothalamic paraventricular nucleus and pituitary-adrenocortical and sympathoadrenal activity: In vivo microdialysis studies. *Front Neuroendocrinol* 16:89–150.
62. Buxton RB, Wong EC, Frank LR (1998) Dynamics of blood flow and oxygenation changes during brain activation: The balloon model. *Magn Reson Med* 39:855–864.
63. Schroeter ML, Cutini S, Wahl MM, Scheid R, Yves von Cramon D (2007) Neurovascular coupling is impaired in cerebral microangiopathy—An event-related Stroop study. *Neuroimage* 34:26–34.
64. Kogler L, et al. (2015) Psychosocial versus physiological stress—Meta-analyses on deactivations and activations of the neural correlates of stress reactions. *Neuroimage* 119:235–251.
65. Amare AT, Schubert KO, Klingler-Hoffmann M, Cohen-Woods S, Baune BT (2017) The genetic overlap between mood disorders and cardiometabolic diseases: A systematic review of genome wide and candidate gene studies. *Transl Psychiatry* 7:e1007.
66. Ashburner J (2007) A fast diffeomorphic image registration algorithm. *Neuroimage* 38:95–113.
67. Behzadi Y, Restom K, Liu J, Liu TT (2007) A component based noise correction method (CompCor) for BOLD and perfusion based fMRI. *Neuroimage* 37:90–101.
68. Tzourio-Mazoyer N, et al. (2002) Automated anatomical labeling of activations in SPM using a macroscopic anatomical parcellation of the MNI MRI single-subject brain. *Neuroimage* 15:273–289.